



Repetitive High-Voltage Pulse Generator Based on Thermally Depolarized Ferroelectrics

Mihai GANCIU¹, Oana CRAMARIUC¹, Andrei Petre SEBE², Răzvan MIRCIOAGĂ³, Andrei LUDU⁴

¹IT Center for Science and Technology, Bucharest, Romania

²Sebit IT Consulting SRL, Bucharest, Romania

³Military Technical Academy, Bucharest, Romania

⁴Embry-Riddle Aeronautical University, Department of Mathematics & Wave Lab,
Daytona Beach, FL 32114, USA

mihai.ganciu@ferrodynamics.com, oana.cramariuc@gmail.com, andrei.sebe@ferrodynamics.com,
razvanmircioaga@gmail.com, andrei.ludu@erau.edu

Abstract: We present a repetitive, non-destructive system for generating high-voltage pulses through fast, controlled thermal depolarization of pre-polarized ferroelectric ceramics. This system represents a significant advance in compact pulsed-power devices, where energy is stored in pre-polarized ferroelectrics. In our device, the ferroelectric pre-polarized ceramic is heated above the Curie temperature in a short, well-defined time interval, releasing the stored electrostatic energy bound by spontaneous polarization as a high-voltage pulse with rise times in the 10–20 ns range, peak amplitudes between 50 and 500 kV, and repetition rates from 0.1 to 10 Hz without material degradation. The system incorporates dedicated subsystems for rapid heating, liquid dielectric insulation, reverse-current blocking, adjustable spark-gap switching, nanosecond-scale diagnostics, and active cooling. Applications include high-power microwave generation, compact X-ray flash radiography, high-power laser pumping, and various medical and industrial sectors requiring compact, reusable pulsed-power sources.

Keywords: ferroelectric pulse generator, thermal depolarization, high-voltage pulse, high-power microwave (HPM).

INTRODUCTION

The generation of high-power electromagnetic pulses remains a critical challenge across multiple domains of modern technology, from inertial confinement fusion to directed energy

applications and advanced diagnostic systems (Altgilbers et al., 2000; Gu et al., 2019; Lysne and Percival, 1975; Neilson, 1957; Setchell, 2005; Shi et al., 2024; Shkuratov et al., 2012; Shkuratov et al., 2014). Traditional capacitor-based pulsed-power systems, while reliable,



face fundamental limitations in energy density and portability that restrict their deployment in field applications and miniaturized systems (Altgilbers et al., 2000; Lysne and Percival, 1975; Neilson, 1957; Setchell, 2005; Shkuratov et al., 2014). Ferroelectric generators (FEGs) offer a compelling alternative by exploiting the rapid depolarization of pre-polarized ferroelectric ceramics to produce ultra-fast, high-voltage pulses in the 100–500 kV range with power outputs reaching gigawatt levels (Altgilbers et al., 2000; Gu et al., 2019; Lines and Glass, 1977; Lysne and Percival, 1975; Neilson, 1957; Scott, 2000; Setchell, 2005; Shi et al., 2024; Shkuratov et al., 2012; Shkuratov et al., 2014).

The operational principle of FEGs relies on mechanically induced phase transitions in ferroelectric materials. When a ferroelectric ceramic such as lead zirconate titanate (PZT) or lead lanthanum zirconate titanate (PLZT) is subjected to shock loading—typically generated by high-explosive detonation—the resulting stress wave drives a rapid transition from the polarized ferroelectric phase to a non-polar or differently oriented state (Altgilbers et al., 2000; Lysne and Percival, 1975; Neilson, 1957; Setchell, 2005; Shkuratov et al., 2014). This shock-induced depolarization releases bound charge at nanosecond timescales, generating electromagnetic pulses with rise times on the order of tens to hundreds of nanoseconds (Agrawal and Bhattacharya, 2014; Haertling, 1999; Lines and Glass, 1977; Zhao et al., 2019). The energy density achievable in these compact systems can exceed that of conventional capacitors by an order of magnitude, with values approaching 1–2 MJ/kg, making FEGs particularly attractive for applications where size, weight, and stored energy are critical constraints (Agrawal and Bhattacharya, 2014; Gu et al., 2019; Potnis et al., 2011; Talantsev et al., 2003).

The relevance of FEGs spans several high-impact technological domains. In fusion energy research, they provide intense electromagnetic fields necessary for magnetic flux compression and fast ignition schemes in inertial confinement fusion (Lines and Glass, 1977; Scott, 2000). Military applications exploit their ability to

generate electromagnetic interference pulses and drive high-power microwave sources. In medical and industrial sectors, FEGs enable compact X-ray flash radiography systems and high-power laser pumping configurations (Gu et al., 2019; Lines and Glass, 1977; Neilson, 1957; Scott, 2000; Shi et al., 2024; Shkuratov et al., 2012). Despite these diverse applications, significant challenges remain in optimizing the coupling between mechanical shock parameters and electrical output characteristics, understanding the complex material response under extreme loading conditions, and developing predictive models that can guide the design of next-generation ferroelectric pulse generators (Lines and Glass, 1977; Scott, 2000).

Explosive FEGs (Agrawal and Bhattacharya, 2014; Haertling, 1999; Ludu et al., 1986; Shkuratov et al., 2005; Talantsev et al., 2003; Zhao et al., 2019) rely on mechanically or detonation-induced depolarization to produce high-voltage pulses in the 50–500 kV range, but they are inherently single-shot, destructive devices that require handling of energetic materials and raise substantial operational safety and logistical issues. Classical work on completely explosive pulsed-power mini-systems and high-explosive pulsed power has identified attractive energy densities but also highlighted constraints related to reusability, test throughput, and integration in civilian laboratories (Lines and Glass, 1977; Scott, 2000).

In parallel, the physics of thermally driven depolarization in ferroelectrics has been extensively studied, with detailed analyses of temperature-dependent spontaneous polarization, domain dynamics, and phase transitions at the Curie temperature T_c in materials such as BaTiO_3 , PZT, and related solid solutions (Agrawal and Bhattacharya, 2014; Haertling, 1999; Lines and Glass, 1977; Zhao et al., 2019). Foundational references (Acosta et al., 2017; Haertling, 1999; Potnis et al., 2011) describe the evolution from historical ferroelectric ceramics toward engineered compositions and domain structures, addressing applications in memories, actuators, and sensors rather than compact pulsed-power generators.



This paper presents a novel approach in the field of FEGs where, instead of obtaining fast depolarization of the ceramic sample using a shock wave, we demonstrate that the same result can be obtained through fast thermal depolarization above the Curie point of the ceramic. The system presented here eliminates the problem of device destruction after each pulse, in addition to providing the benefits of a safe working environment without the use of high explosives. Furthermore, by introducing a procedure of rapid forced cooling, we increase the repetition rate to 10 pulses per second.

The paper is organized as follows: in Section 2, we present the theoretical background and the physical processes of depolarization by shock waves and thermal wavefronts. Section 3 describes the system architecture. Section 4 describes the process of rapid heating and reverse-current blocking, while Section 5 describes the spark-gap switching systems. The full operating cycle is described in Section 6, and an example of experimental realization is introduced in Section 7. In Section 8 (Conclusions), we present a comparison with explosive FEGs, discuss various limitations, and provide examples of applications and other possible advanced architectures.

THEORETICAL BACKGROUND ON THERMAL DEPOLARIZATION

Ferroelectric materials exhibit a non-zero spontaneous polarization below T_c , associated with a symmetry-broken crystal structure and the presence of polar domains separated by domain walls (Haertling, 1999; Lines and Glass, 1977; Zhao et al., 2019). As the temperature approaches T_c from below, the magnitude of spontaneous polarization decreases rapidly, and at T_c the material undergoes a ferroelectric-to-paraelectric phase transition in which long-range polar order vanishes, releasing the energy stored in the ordered domain configuration.

The depolarization of ferroelectric material by a shock wave is a complex process involving several interrelated physical mechanisms at the molecular/atomic scale (Agrawal and

Bhattacharya, 2014; Altgilbers et al., 2000; Gu et al., 2019; Lysne and Percival, 1975; Neilson, 1957; Setchell, 2005; Shi et al., 2024; Shkuratov et al., 2012; Shkuratov et al., 2014; Talantsev et al., 2003; Zhao et al., 2019). On one hand, a shock wave creates an intense, rapid pressure pulse that mechanically distorts the crystal lattice, reorients dipole moments, and switches domains to energetically favorable orientations. Sufficiently strong shock compression also drives the material through phase transitions, causing the ferroelectric to lose polar symmetry above a critical pressure analogous to the Curie temperature effect. On the other hand, shock compression generates significant heating through plastic work and compression. This temperature rise reduces spontaneous polarization (approaching the Curie point) and increases thermal fluctuations that can randomize dipole orientations. The net result is typically a substantial loss of the macroscopic polarization that was present before the shock wave arrived, converting the stored electrostatic energy into charge flow (the depoling current) (Rosenthal et al., 2020). Consequently, detonation-induced depolarization not only destroys the entire system and prevents any repeatability of the experiment with the same sample, but the depolarization mechanism appears to be primarily mechanically stress-driven disruption, where thermal (Curie point) depolarization by phase transition is a secondary effect (Agrawal and Bhattacharya, 2014; Potnis et al., 2011; Talantsev et al., 2003; Zhao et al., 2019).

In contrast, thermal depolarization at the Curie temperature is fundamentally a thermodynamic phase transition driven by the competition between ordering energy and thermal entropy. Below the Curie temperature T_c , in the ferroelectric phase, the free energy of the sample has multiple equivalent minima corresponding to different polarization directions, and thermal fluctuations cannot spontaneously depolarize the material. In Landau-Devonshire theory (Acosta et al., 2017; Potnis et al., 2011; Scott, 2000), the spontaneous polarization P minimizes the expression of the free energy

$$F(P, T) = F_0 + \alpha_0 (T - T_c)^2 + \beta P^4 + \gamma P^6 + \dots$$

with temperature-dependent coefficients (Acosta et al., 2017; Haertling, 1999; Lines and Glass, 1977; Potnis et al., 2011). When temperature exceeds the Curie point T_c , thermal energy disrupts the cooperative alignment interactions between dipoles, and the material undergoes a first-order phase transition to a non-polarized paraelectric phase. Unlike shock depolarization which fragments ferroelectric domains chaotically, thermal depolarization causes domains to simply cease to exist as meaningful entities, and the entire material uniformly transitions to the paraelectric state, where there are no preferred polarization directions. The key distinction from shock depolarization is that the pure thermal process is an equilibrium thermodynamic transition where the system smoothly evolves to minimize free energy, rather than a non-equilibrium mechanical disruption of an otherwise stable state.

However, by selecting compositions with Curie temperatures in the 300–420 K range and a narrow transition window of 10–30 K, such as $Ba_{0.87}Sr_{0.13}TiO_3$, $Ba_{0.88}Sr_{0.12}TiO_3$, $Ba_{0.90}Ca_{0.10}TiO_3$, $BaTi_{0.92}Sn_{0.08}O_3$ (BTS-8), or $Ba_{0.80}Pb_{0.20}TiO_3$ (BPT-20), the change in spontaneous polarization can be made abrupt and well localized in temperature (Acosta et al., 2017; Potnis et al., 2011). When such a body is pre-polarized and then heated rapidly through T_c under open-circuit or quasi-open-circuit conditions, the resulting depolarization manifests as a sharp rise in terminal voltage, which can be harvested

as a high-voltage pulse (Acosta et al., 2017; Haertling, 1999; Lines and Glass, 1977; Potnis et al., 2011; Zhao et al., 2019).

SYSTEM ARCHITECTURE

The proposed FEG device consists mainly of a cylindrical polarized ferroelectric element with high-electrical-conductivity metal depositions (electrodes) on its lids, submerged in a liquid dielectric bath (see Fig. 1). In addition, we place a rapid heating system coaxial to the ferroelectric element and an active cooling assembly. In this way, a thermal pulse generated by the heating device depolarizes the ferroelectric sample, and the free electric charge is collected from the electrodes. As soon as the depoling current is collected into an electric load, and even while the sample is still warm above the Curie point, a continuous DC potential is immediately applied from an external source to the same probe electrodes, inducing a realignment field on the dipoles. Simultaneously, a fast-cooling system activates. This system consists of two symmetrically placed Peltier elements attached to the container (see Fig. 1) and two micro-turbine pumps that induce forced convection in the surrounding dielectric liquid. When the temperature drops below the Curie point, the sample is repolarized and ready for the next discharge. Additionally, the system contains a reverse-current blocking circuit, an adjustable spark-gap switch, and a high-bandwidth measurement and triggering subsystem.

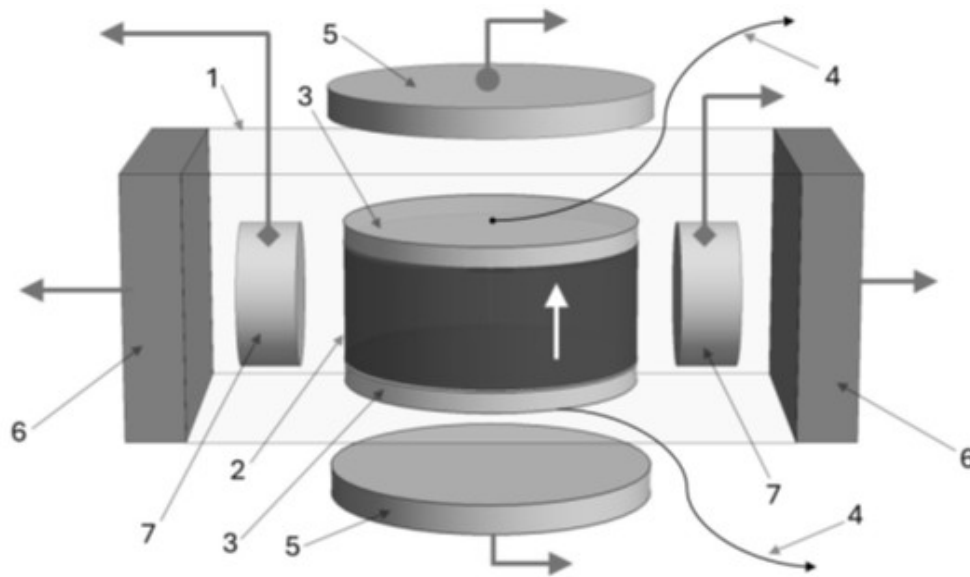


Figure 1. The components of the pulse generator: In a silicone oil container (1), we place the pre-polarized ferroelectric sample with cylindrical geometry (2), where the axial polarization vector is indicated by the white arrow. The ferroelectric disk has surface depositions of high-electrical-conductivity metals (3) on its lids from which electrical terminals (4) are soldered. Two micro-turbine pumps (7) and two symmetrically placed cooling solid-state Peltier elements (6) ensure fast and uniform re-cooling of the sample (3). The ferroelectric is depolarized in a controlled thermal shock by two symmetrically placed lattices of IR lasers (LEDs, 5).

For experimental purposes, the ferroelectric element is typically a disk of BaTiO_3 -based or PZT-type ceramic with a diameter of 20–40 mm and a thickness of 10–25 mm, metallized on opposite faces with Ag or Pt layers and bonded to copper electrodes for low-inductance connections. The body is pre-polarized at electric fields on the order of 3 kV/mm, either in a dedicated step at elevated temperature or by maintaining a DC bias during operation, ensuring a high initial level of remanent polarization around $40 \mu\text{C}/\text{cm}^2$.

The ferroelectric element is immersed in a liquid dielectric such as silicone oil (e.g., Dow Corning 200, 10 cSt), which provides high dielectric strength, uniform heat transfer, and mechanical protection in a stainless-steel vessel with at least one transparent face for optical access. The oil volume, typically between 5 and 50 L, is managed through filtration and temperature control in the 15–60 °C range to guarantee stable electrical and thermal properties.

RAPID HEATING AND REVERSE-CURRENT BLOCKING

Fast thermal excitation is achieved using three alternative or combined approaches: resistive heating, optical heating, or hybrid heating. In the resistive option, a thin Ni-Cr foil of 50–100 μm thickness is attached to one electrode and driven by low-voltage, high-power DC sources (10–50 V, up to several hundred watts), enabling heating rates in the 0.5–10 K/ms range and, for optimized geometries, up to 10–100 K/ms. Optical heating employs xenon flash lamps, halogen lamps, or IR diode laser arrays, either coupled through the dielectric liquid or via optical fibers, providing flexible spatial and temporal control of the heat flux. A hybrid configuration combines IR and visible radiation to tailor the thermal front, improving uniformity and minimizing thermal gradients and mechanical stress in the ceramic body.

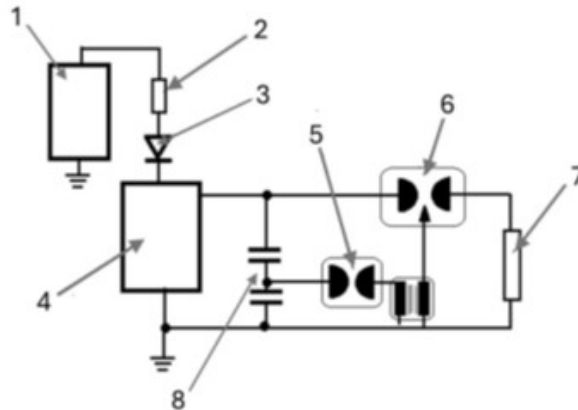


Figure 2. The electrical diagram of the system. The ferroelectric sample (1) generates the high-voltage pulse through a limiting resistor (2) and a protective diode stack (3) into the ferroelectric thermal module (4). Spark-gap switches (5, 6) and capacitive dividers (8) ensure fast switching of the high-voltage pulse to the load (7).

The reverse-current blocking circuit is implemented as a stack of one to 30 high-voltage diodes connected in series with the ferroelectric element and the DC polarization source, dimensioned for up to 500 kV reverse bias and leakage currents on the order of tens of microamperes (Fig. 2). This stack prevents back-discharge into the polarization supply when the depolarization-induced voltage overshoots the DC level, while allowing normal charging currents during polarization and between pulses.

SPARK-GAP SWITCHING AND DIAGNOSTICS

Energy transfer to the external load is controlled by a main spark-gap switch (Ganciu et al., 2007; Ludu et al., 1986; Shkuratov et al., 2005) with adjustable electrode spacing between 1 and 15 mm, using electrode materials such as tungsten, copper, or stainless alloys in gases like dry air or SF₆ at pressures from 0.5 to 5 atm (see Fig. 2). The device can operate in self-breakdown mode when the ferroelectric voltage exceeds the gas breakdown threshold or in trigger mode via an auxiliary spark-gap and a pulse transformer, using a high-voltage pulse generator such as in (Ganciu et al., 2007) or future optical triggering schemes (Rosenthal et al., 2020; Wang et al., 2009).

The diagnostic subsystem comprises at least two capacitive voltage dividers connected in parallel with the ferroelectric and/or the load: a slow, high-ratio divider for DC and low-frequency monitoring, and a fast, nanosecond-response divider for capturing the pulse waveform. Signals are recorded with digital oscilloscopes in the 200 MHz–1 GHz bandwidth and 1–10 GS/s sampling rate, while a programmable logic controller or equivalent coordinates threshold detection, trigger generation, and safety interlocks.

OPERATING CYCLE

A typical operating cycle begins with preparation and polarization, where the ferroelectric element is brought to a temperature below T_c and polarized either in a separate pre-poling process or by connecting a DC high-voltage supply through the resistor-diode chain. In the subsequent heating phase, the resistive or optical heating subsystem is activated to drive the element temperature across T_c within a target time window of 60–300 ms, during which the terminal voltage rises from a baseline of around 40 kV to a maximum in the 50–500 kV range, depending on material and geometry. As the ferroelectric voltage approaches a predefined fraction of



the expected peak (for example, 90%), the fast capacitive divider and comparator generate a trigger signal that initiates conduction in the main spark-gap, often via an auxiliary trigger circuit, thereby connecting the ferroelectric to the external load. The resulting high-voltage pulse exhibits rise times of 10–20 ns and full-width at half-maximum durations of 120–200 ns, delivering the stored energy to loads that may include resistive terminations, nonlinear transmission lines, or high-power microwave (HPM) structures. After each discharge, the cooling subsystem—combining natural convection in the oil, forced circulation at flows on the order of 10 L/min, and Peltier modules in advanced configurations—reduces the ferroelectric temperature back below T_c within tens of seconds, enabling repetition rates from 0.1 to several hertz depending on design. Material repolarization can be performed periodically to compensate for any gradual reduction in remanent polarization, although experimental results indicate stable operation over hundreds to a thousand cycles without significant degradation.

EXPERIMENTAL REALIZATIONS

In a first demonstrative configuration, a pre-polarized BaTiO₃-derived ceramic (e.g., BTS-8 or BPT-20) with a diameter of approximately 50 mm and a thickness of 5–15 mm is heated resistively by a 100 μ m Ni-Cr foil in a 5 L silicone oil tank with two transparent windows. The system uses one or more series high-voltage diodes with microampere-level leakage currents, an adjustable air or nitrogen spark-gap, and a 50 Ω resistive load for monitoring, together with a GHz-class oscilloscope and capacitive divider.

For heating rates around 50 K/ms and repetition rates near 1 Hz, expected results include peak voltages of 50–85 kV on the load, rise times of 10–15 ns, pulse energies consistent with 60–75% energy transfer efficiency, and stable performance over up to 1000 cycles without visible microcracking, delamination, or loss of bulk resistivity. Thermal measurements with K-type thermocouples at multiple radial positions and electrical measurements of amplitude, rise time, jitter, and repetition rate provide a comprehensive characterization of the system dynamics. First experimental results are presented in figure 3.

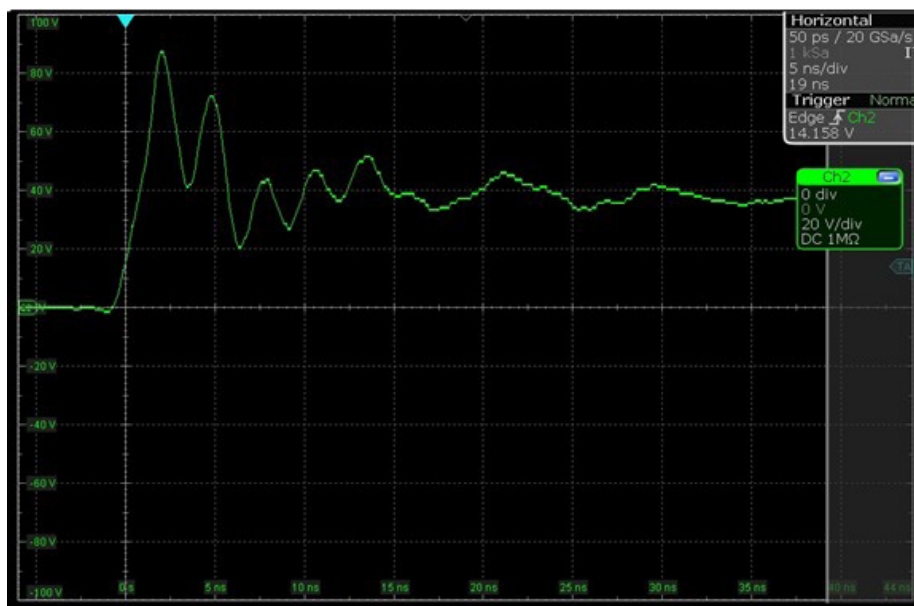


Figure 3. Typical experimental voltage waveform across 0.5 Ohm resistor in series with 50 Ohm load resistor. Voltage is measured with a homemade 1:100 voltage probe coupled with 1:10, 500 MHz probe on RTE 1054, 500 MHz Rhode&Schwarrz oscilloscope.

A second configuration explores continuous polarization, where an initially unpoled BaTiO₃-based element is continuously biased at approximately 40 kV via a resistor and diode stack, while heating is provided by a 550 W IR LED or lamp. In this regime, reported or expected performance includes 70–80 kV peak output, rise times of 10–15 ns, and repetition rates from 0.5 to 2 Hz, with material integrity verified by SEM inspection and remanent polarization measurements after hundreds of cycles.

CONCLUSIONS

In this paper, we introduce a new type of FEG based on a controlled thermal depolarization process. The major advance of such a system consists of its non-destructive, controllable, and repetitive generation of high-voltage pulses from ferroelectric ceramics. By combining fast thermal control, robust reverse-current protection, adjustable spark-gap switching, high-bandwidth diagnostics, and forced cooling, the system can deliver reusable high-voltage pulses suitable for integration into compact infrastructures. Its key advantage over known explosive FEG technologies lies in the non-explosive, safe, and repeatable nature, which opens new possibilities in industrial testing and scientific research (including medical fields) where high-performance electromagnetic sources must coexist with stringent safety and reusability requirements.

Compared to explosive ferroelectric pulsed-power systems, the present generator eliminates detonation and mechanical shock, relying instead on a purely thermal stimulus to trigger depolarization. This transition from explosive to controlled thermal depolarization removes the need for explosives handling, drastically improves operator and facility safety, and enables multi-shot, laboratory-friendly operation with programmable timing and repetition frequency.

Nevertheless, current implementations are limited to pulse amplitudes in the 50–500 kV range, below those achievable with large Marx generators or some high-explosive single-shot devices, and require non-negligible

thermal management resources to sustain high repetition rates between 1 and 10 Hz. Mass, volume, and power-budget constraints must also be addressed for deployment on mobile platforms, where compactness, ruggedness, and autonomous operation are paramount.

Future developments of this project may include stacking multiple ferroelectric elements in series to increase output voltage, using parallel architectures to shape current and impedance, and exploring alternative geometries such as toroidal, ring-like, or segmented elements with multiple anodes to improve energy density and field uniformity. Hybrid depolarization schemes that combine thermal loading with mechanical compression or femtosecond-scale laser excitation are also envisioned to achieve sub-10-ns voltage rise times.

The synthesis of new ferroelectric materials tailored to this application is required, featuring a stable Curie temperature of approximately 80°C and a sharp drop in the dielectric constant by a factor of 15–20 from its maximum value over a temperature range of 10–20 K, leveraging recent advances in the use of artificial intelligence for the design of novel ferroelectrics (Zhang and Chen, 2025)

At the system level, the ferroelectric thermal depolarization generator may serve as a primary high-voltage source for an explosively pumped flux compression generator, followed by a vircator-based X-band stage and a polarization-controlled antenna. Target system parameters involve 100–500 kV input pulses with 10–50 ns rise time, 1–10 GW pulsed microwave output in the 8–12 GHz band, pulse durations of 10–100 ns, and jitter on the order of 10 ns, satisfying demanding requirements for research and defense electromagnetic applications. Practical applications range from electromagnetic jamming and temporary disruption of communications, navigation, and radar systems to durability testing of electronics under high-power electromagnetic pulse environments, high-power radar and ground-penetrating sensing, non-lethal neutralization of drones and autonomous vehicles, as well as plasma initiation and ultra-fast ionization and particle acceleration studies.



ACKNOWLEDGEMENTS

This work is related to OSIM patent application A/00573, November 28, 2025.

REFERENCE LIST

- Acosta, M. et al. (2017) BaTiO₃-based piezoelectrics: fundamentals, current status, and perspectives, *Applied Physics Reviews*, 4(4), p. 041305.
- Agrawal, V. and Bhattacharya, K. (2014) Shock wave propagation through a model one-dimensional heterogeneous medium, *International Journal of Solids and Structures*, 51(21–22), 3604–3618. Available at: <https://www.sciencedirect.com/science/article/pii/S0020768314002534> [Accessed 27 April 2026].
- Altgilbers, L.L., Brown, M.D.J., Grishnaev, I. et al. (2000) *Magnetocumulative Generators*. New York: Springer-Verlag.
- Freeman, L. (2016) *Method for Derivation and Synthesis of Electromagnetic Environmental Effects Requirement Limits for Achieving System Level Electromagnetic Compatibility*. PhD thesis. University of Central Florida. Available at: <https://stars.library.ucf.edu/etd/5215/> [Accessed 27th April 2026].
- Ganciu, M. et al. (2007) U.S. Patent No. 7,927,466 B2. Available at: <https://patents.google.com/patent/US7927466B2/zh> [Accessed 27th April 2026].
- Gu, Y.-J., Jirka, M., Klimo, O. and Weber, S. (2019) Gamma photons and electron-positron pairs from ultra-intense laser-matter interaction: a comparative study of proposed experiments, *Matter and Radiation at Extremes*, 4(6), p. 064403. Available at: <https://pubs.aip.org/aip/mre/article/4/6/064403> [Accessed 27th April 2026].
- Haertling, G.H. (1999) Ferroelectric ceramics: history and technology. *Journal of the American Ceramic Society*, 82(4), 797–818.
- Lines, M.E. and Glass, A.M. (1977) *Principles and Applications of Ferroelectrics and Related Materials*. Oxford: Oxford University Press.
- Ludu, A., Nicolau, P. and Novac, B. (1986) Explosive plasma gun pulsed power systems, in Fowler, C.M., Caird, R. and Erikson, D.J. (eds.) *Megagauss Magnetic Field Generation and Related Topics*. New York: Plenum Press, 369–375.
- Lysne, P.C. and Percival, C.M. (1975) Electric energy generation by shock compression of ferroelectric ceramics: normal-mode response and Curie-point phase transition, *Journal of Applied Physics*, 46(4), 1519–1525.
- Neilson, F.W. (1957) Effects of strong shocks in ferroelectric materials. *Bulletin of the American Physical Society*, 2(9), p. 302.
- Potnis, P.R., Tsou, N.-T. and Huber, J.E. (2011) A review of domain modelling and domain imaging techniques in ferroelectric crystals. *Materials*, 4(2), 417–447.
- Rosenthal, E.W. et al. (2020) Collection of remote atmospheric data via femtosecond filament plasma fluorescence spectroscopy. *Optics Express*, 28(17), p. 24599.
- Scott, J.F. (2000). *Ferroelectric Memories*. Berlin: Springer.
- Setchell, R.E. (2005) Refractive-index measurements of sapphire, PMMA, and fused silica in stress waves. *Journal of Applied Physics*, 97(1), p. 013507.
- Shi, P., Liu, J., Song, Y., Wu, W., Liu, L., Zhou, X., Chen, X., Lou, X., and Liu, P. (2024) Ferroelectric ceramics for shock-driven pulsed power. *Journal of Applied Physics*, 135(12), p. 124103. Available at: <https://pubs.aip.org/aip/jap/article/135/12/124103/3278945> [Accessed 27th April 2026].
- Shkuratov, S.I. et al. (2005) Completely explosive ultracompact high-voltage pulse generating system. in *Proceedings of the 2005 IEEE Pulsed Power Conference*. IEEE, pp. 1095–1098.
- Shkuratov, S.I., Baird, J., Talantsev, E.F. et al. (2012) Spontaneous depolarization of PZT 95/5 ferroelectric ceramics in the body of a shock wave. *Scientific Reports*, 2, p. 931.
- Shkuratov, S.I., Baird, J., Antipov, V.G. et al. (2014) Depolarization of hard and soft piezoelectric ceramics by a shock wave. *Applied Physics Letters*, 104(21), p. 212901.
- Talantsev, E.F. et al. (2003) Compact explosive-driven sources of powerful electromagnetic pulses, *Review of Scientific Instruments*, 74(1), pp. 225–232.



- U.S. Patent No. 4,845,378 A (1989). Available at: <https://patents.google.com/patent/US4845378A/en> [Accessed 27th April 2026].
- Wang, J. et al. (2009) Experimental research on repetitive nanosecond-pulse laser-triggered spark gap switches with UV preionization, *IEEE Transactions on Dielectrics and Electrical Insulation*, 16(4), pp. 956–961.
- Wilson, C. (2008) High Altitude Electromagnetic Pulse (HEMP) and High Power Microwave (HPM) Devices: Threat Assessments. Technical Report No. CRSRL32544, ADA529982. Defense Technical Information Center.
- Zhang, C. and Chen, X. (2025) 'FerroAI: a deep learning model for predicting phase diagrams of ferroelectric materials', *npj Computational Materials*, 11, p. 282. Available at: <https://doi.org/10.1038/s41524-025-01778-0> [Accessed 27th April 2026].
- Zhao, D. et al. (2019) Depolarization of ultrathin ferroelectric PbZr_{0.2}Ti_{0.8}O₃ films under finite electrical boundary conditions. *Nature Communications*, 10, p. 3177.



This is an open access article distributed under the terms and conditions of the Creative Commons Attribution-NonCommercial 4.0 International License.